

Robust initialization of 2D-3D image registration using the projection-slice theorem and phase correlation

M. J. van der Bom^{a)} and L. W. Bartels

Image Sciences Institute, University Medical Center Utrecht, QOS.459, P.O. Box 85500, 3508 GA Utrecht, The Netherlands

M. J. Gounis

Department of Radiology, University of Massachusetts Medical School, 55 Lake Avenue North, H2-573, Worcester, Massachusetts 01655

R. Homan and J. Timmer

Philips Healthcare, X-Ray Predevelopment, P.O. Box 10000, 5680 DA Best, The Netherlands

M. A. Viergever and J. P. W. Pluim

Image Sciences Institute, University Medical Center Utrecht, QOS.459, P.O. Box 85500, 3508 GA Utrecht, The Netherlands

(Received 11 September 2009; revised 4 February 2010; accepted for publication 25 February 2010; published 30 March 2010)

Purpose: The image registration literature comprises many methods for 2D-3D registration for which accuracy has been established in a variety of applications. However, clinical application is limited by a small capture range. Initial offsets outside the capture range of a registration method will not converge to a successful registration. Previously reported capture ranges, defined as the 95% success range, are in the order of 4–11 mm mean target registration error. In this article, a relatively computationally inexpensive and robust estimation method is proposed with the objective to enlarge the capture range.

Methods: The method uses the projection-slice theorem in combination with phase correlation in order to estimate the transform parameters, which provides an initialization of the subsequent registration procedure.

Results: The feasibility of the method was evaluated by experiments using digitally reconstructed radiographs generated from *in vivo* 3D-RX data. With these experiments it was shown that the projection-slice theorem provides successful estimates of the rotational transform parameters for perspective projections and in case of translational offsets. The method was further tested on *ex vivo* ovine x-ray data. In 95% of the cases, the method yielded successful estimates for initial mean target registration errors up to 19.5 mm. Finally, the method was evaluated as an initialization method for an intensity-based 2D-3D registration method. The uninitialized and initialized registration experiments had success rates of 28.8% and 68.6%, respectively.

Conclusions: The authors have shown that the initialization method based on the projection-slice theorem and phase correlation yields adequate initializations for existing registration methods, thereby substantially enlarging the capture range of these methods. © 2010 American Association of Physicists in Medicine. [DOI: [10.1118/1.3366252](https://doi.org/10.1118/1.3366252)]

Key words: 2D-3D registration, projection-slice theorem, image-guided interventions, x-ray guidance, 3-dimensional rotational x-ray

I. INTRODUCTION

Image-guided procedures which include image-guided radiation therapy, image-guided surgery, and image-guided minimally invasive therapy are navigated by image data acquired during the procedure. Real-time visualization during these procedures is commonly done by 2D x-ray imaging. The downside of this imaging technique is that the perspective images do not provide 3D information. Additionally, some soft tissues that can be visualized using 3D imaging techniques are not visible in 2D x-ray imaging. Incorporating preinterventional/preoperative 3D volume data, obtained for diagnosis and/or treatment planning, into the workflow of image-guided procedures would therefore lead to 3D insight and improved visualization of anatomical structures.

In order to enable the use of preinterventional data and intrainerventional data in the same reference frame, the relationship between the preinterventional coordinate system and the patient must be determined during the procedure. One way to do this directly is by image-to-patient registration. Registration is performed by manually matching corresponding points (e.g., markers or anatomical landmarks) that are located on the patient and are also present in the 3D volume data loaded into navigation machinery.^{1,2} Another method, referred to as registration-free or direct navigation, obtains a new 3D volume as soon as the patient is positioned in the interventional suite. Because the 3D volume is obtained on a calibrated system, the exact relation between vol-

ume and patient are known. By 3D-3D registration, any pre-interventional volume can be used during the procedure.³⁻⁵

The downside of both methods is that patient motion results in the loss of the relation between the patient and the 3D volume, which can be recovered by navigation machinery⁶ or by repeating the registration procedure or by acquiring a new 3D volume. The use of navigation machinery during procedures provides good accuracy; however, an intervention room might not always supply enough space for such machinery. In addition, performing multiple manual registrations is time-consuming as is the repeated acquisition of additional 3D data. More importantly, the latter exposes the patient to an increased amount of radiation when 3D imaging is based on x-rays.

A third method to obtain a patient-volume relation that does not require navigation machinery or additional 3D imaging is 2D-3D image registration.⁷⁻⁴⁶ Here, patient-volume relation is determined indirectly by registering 2D projection images of the patient acquired during the intervention to the preoperative 3D volume. Over the past two decades, various 2D-3D image registration methods have been proposed.

Although very accurate 2D-3D registration methods are available, they are often limited by a small capture range. The registration will not be successful when the initial mis-registration lies outside the capture range that is specific to the method applied. Maximal initial offsets leading to successful registrations reported previously are in the order of 1 mm mean target registration error (mTRE) when one x-ray image is used and 4–11 mm mTRE when two oblique x-ray images are used.^{37,43,46,47} The capture range was defined as the 95% success range and success as a final mTRE smaller than 2 mm.

The objective of the research reported in this paper was to develop a method that provides a large capture range. We have investigated the possibility to give a fast and robust estimate of the transform parameters as an initialization for a more accurate 2D-3D registration method. The proposed initialization method is based on the projection-slice theorem and phase correlation. It performs a slice-to-volume registration on the Fourier spectra of 2D projection images and the Fourier spectrum of a 3D data set acquired of the same object in order to estimate the pose of the 3D data set relative to the projection images. Subsequently, the translational offset is estimated by phase correlation. With this method we aim to estimate the transform parameters to reduce the total mTRE to a value that lies within the limited capture range of existing registration methods with high accuracy. Fourier-based methods^{48,49} and phase correlation^{50,51} have been well explored for 2D-2D and 3D-3D registration. Preliminary results on using the projection-slice theorem were presented in Van der Bom *et al.*⁵² and a similar method was proposed later on by Zosso *et al.*⁵³ It should be noted that, due to reasons discussed in this paper, our method was developed to provide an approximation of the registration parameters and complete convergence is left to a 2D-3D registration method. The feasibility of the approach was tested in experiments on both *in vivo* and *ex vivo* data.

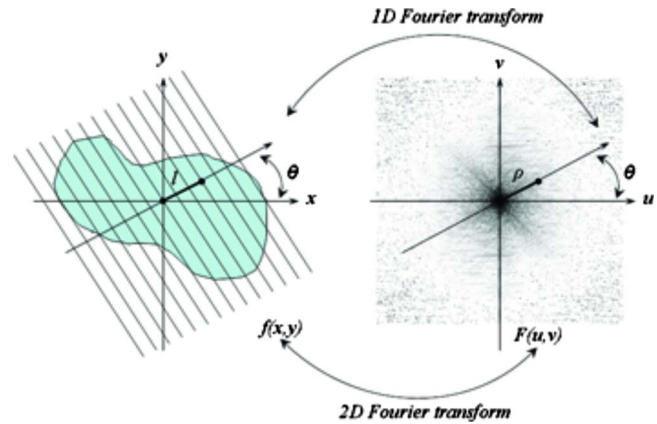


FIG. 1. Schematic overview of the projection-slice theorem.

II. MATERIALS AND METHODS

II.A. Projection-slice theorem

The projection-slice (also known as the Fourier-slice or central-slice) theorem⁵⁴ defines a relationship between the Fourier spectrum of an N -dimensional function and the Fourier spectra of its $(N-1)$ -dimensional projections. In this section we recapitulate this theorem for a 2D object and its 1D projections. The parallel projection $p_{\theta}(l)$ of an object $f(x,y)$ on a line through the origin with angle θ relative to the x -axis evaluated at a distance l from the origin (see Fig. 1) can be written as

$$p_{\theta}(l) = \int_{-\infty}^{\infty} \int_{-\infty}^{\infty} f(x,y) \delta(x \cos \theta + y \sin \theta - l) dx dy, \quad (1)$$

where δ is the Dirac delta function. The Fourier transform of $f(x,y)$ with respect to x and y is given by

$$F(u,v) = \int_{-\infty}^{\infty} \int_{-\infty}^{\infty} f(x,y) e^{-i2\pi(ux+vy)} dx dy \quad (2)$$

and the Fourier transform $P_{\theta}(\rho)$ of $p_{\theta}(l)$ with respect to l is

$$P_{\theta}(\rho) = \int_{-\infty}^{\infty} p_{\theta}(l) e^{-i2\pi\rho l} dl. \quad (3)$$

Substituting Eq. (1) into Eq. (3) gives

$$\begin{aligned} P_{\theta}(\rho) &= \int_{-\infty}^{\infty} \int_{-\infty}^{\infty} \int_{-\infty}^{\infty} f(x,y) \delta(x \cos \theta + y \sin \theta - l) \\ &\quad \cdot dx dy \cdot e^{-i2\pi\rho l} dl \\ &= \int_{-\infty}^{\infty} \int_{-\infty}^{\infty} f(x,y) e^{-i2\pi\rho(x \cos \theta + y \sin \theta)} dx dy, \end{aligned} \quad (4)$$

from which we can distill the identity known as the projection-slice theorem

$$F(\rho \cos \theta, \rho \sin \theta) = P_{\theta}(\rho). \quad (5)$$

Specifically, the projection-slice theorem states that the one-dimensional Fourier transform of a projection $p_{\theta}(l)$ of a two-dimensional function $f(x,y)$ equals the spectrum found along

a line at angle θ in the two-dimensional Fourier transform of the function $f(x, y)$ (see Fig. 1). Because of the validity of this theorem in n dimensions⁵⁵ we can extend this relation to the 2D-3D case to find the rotational transform parameters between a 3D volume and a 2D orthoscopic projection of that volume. Hence, the 2D Fourier transform of a projection $P_{\theta, \varphi, \gamma}(u_P, v_P)$, with projection angles $(\theta, \varphi, \gamma)$ and (u_P, v_P) the coordinates in the projection plane, is identical to the spectrum on the 2D plane described by the normal with Euler angles θ and φ and γ going through the origin in the 3D Fourier transform of the 3D data.

II.B. Phase correlation

Phase correlation is a registration technique that is based on the Fourier shift theorem which states that a shift in the spatial domain corresponds to a phase difference in the frequency domain. Let F_1 and F_2 be the Fourier transforms of two images f_1 and f_2 , respectively, that are shifted by m and n with respect to each other

$$f_2(x, y) = f_1(x - m, y - n). \quad (6)$$

The Fourier shift theorem is then given by

$$F_2(u, v) = e^{-i2\pi(um+vn)} F_1(u, v). \quad (7)$$

The phase difference between $F_1(u, v)$ and $F_2(u, v)$ can be calculated using the cross-power spectrum $C(u, v)$, defined as

$$C(u, v) = \frac{F_1(u, v) F_2^*(u, v)}{|F_1(u, v) F_2^*(u, v)|} = e^{i2\pi(um+vn)}, \quad (8)$$

where $F_2^*(u, v)$ is the complex conjugate of $F_2(u, v)$. The inverse Fourier transform $c(x, y)$ of $C(u, v)$ is a Kronecker delta function that indicates the relative shift between the images

$$c(x, y) = \delta(x + m, y + n). \quad (9)$$

II.C. Projection-slice theorem and phase correlation based initialization of 2D-3D image registration

A 2D-3D registration problem involves ten transform parameters which can be divided into two groups. The first group are the extrinsic parameters that contains the six 3D-3D rigid body transformation parameters which describe the position and orientation of the 3D volume. The second group are the intrinsic parameters that contains information on the focal distance (the distance from the source to the projection plane), the position of the projection plane with respect to the object, and the pixel size of the projection plane. Usually in a 2D-3D registration problem the intrinsic parameters are known and the extrinsic parameters need to be optimized. Our method uses the projection-slice theorem to estimate the orientation (defined by the Euler angles θ , φ , and γ) of the 3D volume that corresponds to a 2D projection image. Let $F(u_F, v_F, w_F)$ and $P(u_P, v_P)$ be the Fourier transforms of the 3D volume $f(x_f, y_f, z_f)$ and a projection $p(x_p, y_p)$, respectively. In order to find the Euler angles E

$= (\theta, \varphi, \gamma)$ that describe the orientation of the 3D volume $f(x_f, y_f, z_f)$ at which the projection $p(x_p, y_p)$ was acquired, we must find the plane $I(u_I, v_I)$ in $F(u_F, v_F, w_F)$ through the center of the volume that has maximal correspondence with $P(u_P, v_P)$. The orientation of that plane is described by the Euler angles we are looking for. Thus,

$$E = \arg \min_{\theta, \varphi, \gamma} D(P, I), \quad (10)$$

where we strive to minimize $D(P, I)$, the function that calculates the difference between the Fourier spectra P and I . We employed a sum of absolute differences similarity measure, applied to the modulus of the Fourier transforms of the 3D volume and the 2D projections. So far we have used continuous functions in our formulations but in practice the 3D volumes and the 2D projection images used are discrete data sets. Therefore the Fourier transforms and the similarity measure were implemented as

$$D(P, I) = \frac{1}{NM} \sum_{j=1}^M \sum_{i=1}^N (|P_{ij}^{\text{mod}} - I_{ij}^{\text{mod}}|). \quad (11)$$

Here, P_{ij}^{mod} and I_{ij}^{mod} denote the i, j th element of the modulus of $P(u_P, v_P)$ and $I(u_I, v_I)$, respectively, with $N \times M$ elements. Planes in the 3D Fourier spectrum were resampled with fixed matrix size and pixel spacing, which were equal to the size and spacing of a coronal slice of the 3D volume data. The similarity function described in Eq. (11) was optimized using Powell's method.⁵⁶

As mentioned earlier, the projection-slice theorem describes the relation between a 3D volume and its 2D orthoscopic projections. In practice, x-ray projection images are acquired with a cone-beam geometry leading to images that are different from those generated with parallel-beam geometry. The proposed method will therefore not converge to the correct rotational parameters. However, assuming the distance from the object to the detector is relatively small compared to the distance from the x-ray focus to the detector, perspective projections will show sufficient similarity with their corresponding orthoscopic projections in order to provide a good estimate of the rotational parameters.

After an estimate of the rotational transform parameters had been obtained, phase correlation was used to estimate the translational transform parameters. The cross-power spectrum was calculated in a discrete manner, leading to an estimated shift expressed in pixels. It appeared that phase correlation obtained using $I(u_I, v_I)$ led to erroneous results because of interpolation artifacts. Therefore, the Fourier transform of an orthoscopic projection, generated using the estimated rotational parameters, was used to calculate the phase correlation. All software was developed using the *ITK Segmentation and Registration Toolkit*.⁵⁷

III. EXPERIMENTS

To test and validate our estimation method we performed three sets of experiments. In the first set of experiments (A) we used digitally reconstructed radiographs to determine the influence of perspective projections and translational offsets

on the estimation of the rotational parameters using the projection-slice theorem. In the second set (B), we tested the complete initialization method, i.e., estimation of the transform parameters using the projection-slice theorem and phase correlation on x-ray data. In the third set of experiments (C), the initialization method was followed by an intensity-based 2D-3D registration algorithm and compared to registration without initialization to test whether the proposed method leads to improved registration success. Because the x-ray data was acquired with a calibrated clinical system, gold standard transformations were available for validation.

III.A. Projection-slice theorem experiments on digitally reconstructed radiographs

A thoracic canine data set was acquired with an x-ray angiography C-arm system (Allura Xper FD20, Philips Healthcare, Best, The Netherlands) in an angiosurgical suite obtained during a spinal surgery. All experiments were approved by the Institutional Animal Care and Use Committee of the University of Massachusetts. Digitally reconstructed radiographs (DRRs) generated with various rotational and translational parameters were registered to their corresponding three-dimensional rotational x-ray (3D-RX) data sets. With these experiments, we quantified the robustness and accuracy of the estimates provided by the projection-slice theorem algorithm as a function of rotational and translational offsets. By using DRRs generated with a point source, the effect of projection with cone-beam geometry on the success of the initialization algorithm assuming parallel projection was tested. Evaluation using DRRs was straightforward because gold standard parameters were known.

In the first experiment, the performance of the method as a function of rotational offsets was tested. DRRs were generated with rotational parameters varying from -20° to 20° with steps of 5° for all three axes of rotation while keeping the translational parameters fixed at 0 mm. In the second experiment the influence of translational offsets was investigated. DRRs were generated with fixed rotational parameters ($\theta = -6^\circ$, $\varphi = 5^\circ$, $\gamma = -4^\circ$) and translational parameters were varied from -10 to 10 mm with steps of 5 mm. The estimation method was started at 0° and 0 mm for all three rotational and translational transform parameters, respectively.

As an error measure we have used the mTRE.⁵⁸ The mTRE was defined as the mean distance between predefined target points in the 3D volume transformed with some arbitrary transformation and with the gold standard transformation, i.e., the transformation corresponding to a perfect registration

$$\text{mTRE}(T) = \frac{1}{N} \sum_{n=1}^N \|T p_n - T_{\text{gold}} p_n\|. \quad (12)$$

Here, N is the total number of target points p_n , T_{gold} is gold standard transformation, and T is a transformation that can for instance be the estimate given by the algorithm or the initial transformation prior to the estimation process. In the

remainder of this paper, the start registration error before the estimation process and the registration error after the estimation process are referred to as $\text{mTRE}_{\text{start}}$ and $\text{mTRE}_{\text{estimate}}$, respectively. In order to evaluate the performance of the estimation of the rotational parameters by the projection-slice theorem as a function of initial translational offset, we calculated the $\text{mTRE}_{\text{estimate}}$ caused by rotational offsets only ($\text{mTRE}_{\text{estimate}}^R$) and the $\text{mTRE}_{\text{start}}$ values caused by translational offsets only ($\text{mTRE}_{\text{start}}^T$). Hence, $\text{mTRE}_{\text{estimate}}^R$ was calculated using Eq. (12) where T contained the rotational parameters estimated by the algorithm and the gold standard translation parameters. Similarly, the calculation of $\text{mTRE}_{\text{start}}^T$ T contained the gold standard rotation parameters and the initial translation parameters. In order to provide a robust initialization for 2D-3D registration methods, our method will have to provide an estimate of the transform parameters within the capture range of these methods. In order to compare our results to those reported by Van de Kraats *et al.*,⁴⁷ we chose to calculate the mTRE values using eight target points located on the vertices of a rectangular region of interest with the same dimensions ($82.65 \times 39.15 \times 82.65$ mm³) as described in the evaluation method in Ref. 47. With these target points, a rotation of 1.0° around one of the three axes will lead to an mTRE of 0.8–1.0 mm. Reported initial misregistrations leading to successful registrations are in the order of 4–11 mm mTRE when two x-ray images are used.^{37,46,47} Estimates with an $\text{mTRE}_{\text{estimate}}$ smaller than 7.5 mm (the average of the reported capture ranges) were considered successful. The capture range was defined as the 95% success range as was proposed in Ref. 47. Parameter settings for the generation of DRRs, such as distance from source to detector (1195 mm), distance from object to detector (385 mm), and detector size (288 mm), were based on those obtained from a calibrated 3D-RX system.

III.B. Initialization experiments on x-ray data

To test the feasibility of the estimation method for clinical application, experiments were performed using x-ray data acquired with a clinical system. Two 3D-RX data sets of a vacuum sealed ovine hind limb were acquired. For the reconstruction of a 3D-RX volume of $256 \times 198 \times 256$ voxels (isotropic voxel size of 0.98 mm³), a set of 116 projection images was acquired for which the rotational x-ray source was rotated 202.5° around the subject around one axis, corresponding to parameter φ in this paper (see Fig. 2). The x-ray images had a resolution of 1024×792 pixels (isotropic pixel size of 0.37 mm²) and were resized to 256×198 pixels. Because the 3D-RX system was calibrated, the intrinsic and extrinsic transform parameters that relate the 3D volume to the projection images were known. Before the second acquisition, the hind limb was manually rotated and translated in order to create an extra offset.

In the 3D-RX data sharp transitions are present that represent the bounding box of the reconstructed volume. In order to exclude the influence of sharp edges the data was masked with a Gaussian blurred ($\sigma = 3$ voxels) binary sphere and a Gaussian blurred ($\sigma = 3$ pixels) binary disk for the 3D

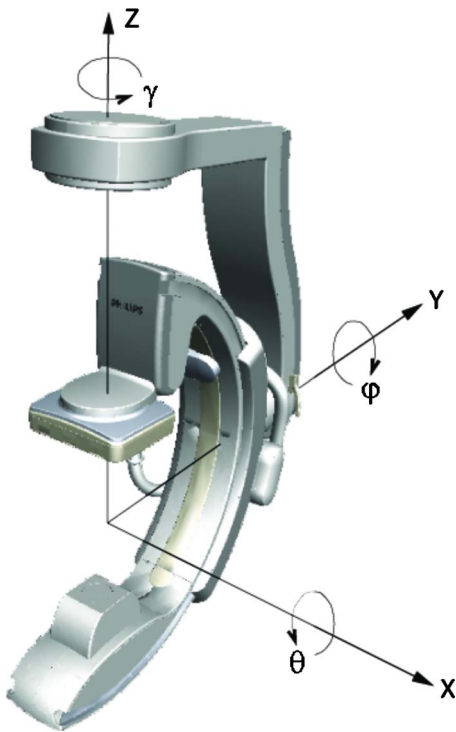


FIG. 2. Schematic overview of the x-ray angiography C-arm system. The coordinate system and the rotational parameters as defined in this article are indicated.

volume and x-ray images, respectively. The sphere and disk had radii of 87 pixels and the center points were located at the center of the volume and image data. Screenshots of 3D volumes and x-ray images are shown in Fig. 3.

From both data sets, 33 adjacent x-ray images were selected that were acquired within an angular difference of approximately 60° . The estimation method was tested using the two sets of x-ray images and both reconstructions. Transform parameters were estimated for all selected x-ray images relative to both reconstructions, thus leading to 132 experi-

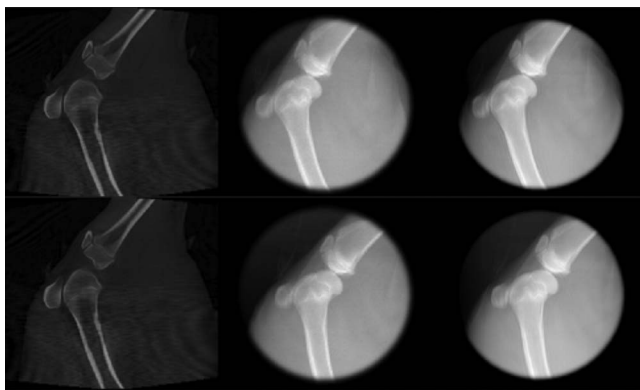


FIG. 3. Data used for experiments (B). Left column: Coronal slices of the 3D-RX data sets. Center column: Anterior-posterior x-ray images that were masked using a Gaussian binary blurred disk. Right column: Anterior-posterior orthogonal projection images obtained with the projection-slice theorem. X-ray and projection images correspond to the 3D-RX data set in the same row.



FIG. 4. Data used for experiments (C) Left: Coronal slice of the 3D-RX data sets of human skull. Center: Masked x-ray image. Right: Orthogonal projection image obtained with the projection-slice theorem.

ments. Experiments were performed three times using different start parameters in order to test the performance of the method for a range of initial offsets.

The transform parameters corresponding to the manual displacement were determined by performing 3D-3D rigid body registration on the reconstructed volumes with *elastix*.⁵⁹ As a result, the gold standard 2D-3D transform parameters for all x-ray images were known.

Mean target registration error before and after the estimation were calculated using Eq. (11). Estimates with a mTRE smaller than 7.5 mm were considered successful. The overall performance of the method was evaluated by calculating the capture range for all x-ray experiments using the definition described in Sec. III A.

III.C. Intensity-based 2D-3D registration experiments on clinical patient data

The method was tested using clinical patient 3D-RX data of a human skull acquired during a neurointervention. For the reconstruction of the 3D-RX volume with a resolution of 256^3 voxels (isotropic voxel size 0.76 mm^3) 116 x-ray images with a resolution of 952^2 pixels (isotropic pixel size of 0.31 mm^2) were obtained.

A single x-ray image was selected, resized to 256^2 pixels and registered to the 3D-RX volume. The selected x-ray image and a coronal slice of the 3D-RX volume are shown in Fig. 4. Registration was performed with an optimized intensity-based 2D-3D registration method (IBM) only. The intensity-based 2D-3D registration algorithm was implemented with a normalized gradient correlation similarity measure^{10,28,39,60} and optimization was performed by Powell's method. Registration experiments were started using randomly generated transform parameters with a frequency of ten sets of start parameters per 1 mm mTRE. Start and final mean target registration errors (mTRE_{start} and mTRE_{final}) were calculated with the same target points as in (A) and (B). The capture range, defined as the 95% success range, of the IBM was determined. Registrations with final mTRE smaller than 2 mm (Ref. 47) were classified as successful. Subsequently, registration experiments were performed with the same intensity-based method with and without using initialization by the projection-slice theorem and phase correlation (I-IBM). Experiments were started with the randomly generated transform parameters with correspond-

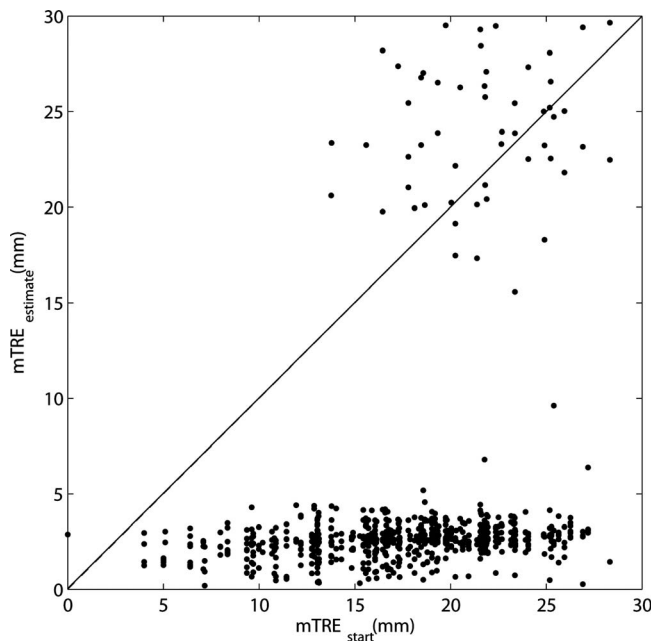


FIG. 5. Results of the projection-slice theorem experiments on DRRs (A). $mTRE_{estimate}$ are given as a function of $mTRE_{start}$. The boundary of no improvement is indicated by the solid line. Initial offsets were caused by rotations around three axes varying from -20° to 20° .

ing $mTRE_{start}$ outside the capture range of the IBM. Prior to performing the initialization method, volume and image data were masked as explained in (B).

IV. RESULTS

IV.A. Projection-slice theorem experiments on digitally reconstructed radiographs

The results of the experiments using digitally reconstructed radiographs are presented in Figs. 5 and 6. Figure 5 shows the results of the experiments with rotational offsets varying from -20° to 20° and 0 mm translational offset. Corresponding $mTRE_{start}$ ranges from 4.0 to 28.3 mm. The solid line indicates where the $mTRE_{estimate}$ is equal to

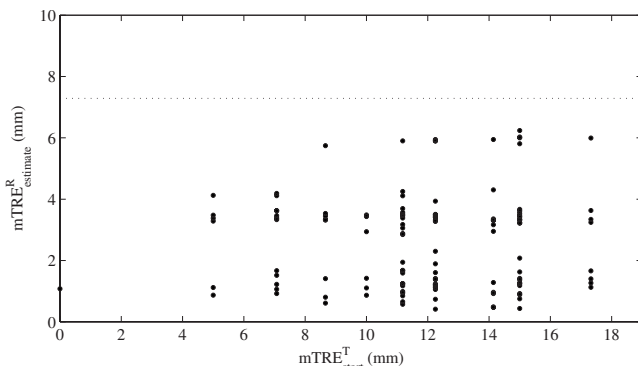


FIG. 6. Results of the projection-slice theorem experiments on DRRs (A). $mTRE_{estimate}^R$ are given as a function of $mTRE_{start}^T$. The line of no improvement is indicated by the dashed line. Initial offsets were caused by fixed rotations around three axes and translations varying from -10 to 10 mm along three axes.

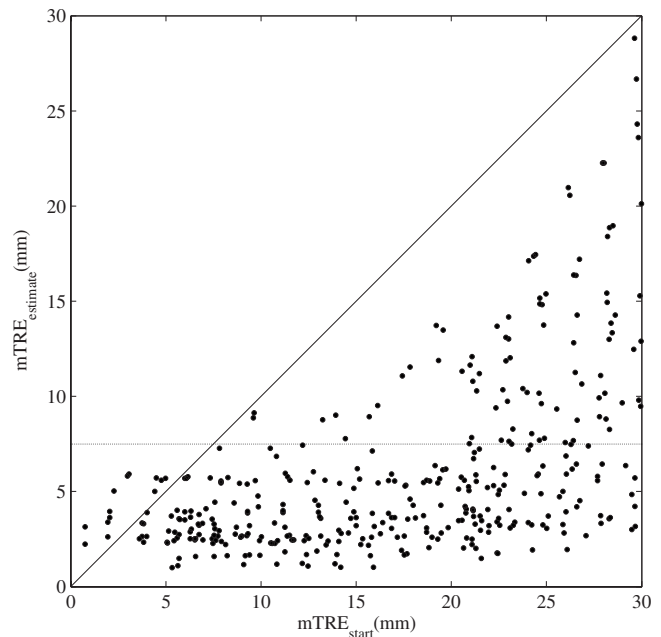


FIG. 7. Results of the initialization experiments (B). $mTRE_{estimate}$ are given as a function of $mTRE_{start}$. The boundary of no improvement and the threshold for success are indicated by the solid and the dashed line, respectively.

$mTRE_{start}$. For points above or on this line our method provides no improved estimate. The estimation method provided a capture range of 19.3 mm. Three outliers (located at $mTRE_{start}$ of 13.78, 20.63, and 21.61 mm) were left out for visibility.

In Fig. 6, the results for the experiments with translational offsets varying from -10 to 10 mm and fixed rotational offsets ($\theta = -6^\circ$, $\varphi = 5^\circ$, and $\gamma = -4^\circ$) are presented. The dashed line in Fig. 6 indicates the $mTRE_{start}^R$ (7.3 mm), i.e., the mean target registration error that resulted from rotational offset only. Values below this line indicate an improved estimate of the rotational parameters. For all experiments the estimation method provided an improvement. In 83.9% of the cases the estimation method gave a reduction of 50% or more of the initial rotational offset.

IV.B. Initialization experiments on x-ray data

In Fig. 7, the results of the x-ray experiments are displayed in terms of mTRE calculated as described in Sec. II. The mTRE after estimation is plotted as a function of the initial mTRE. The boundary of no improvement is indicated by the dashed line and the boundary for success is indicated by the solid line. The capture range of the estimation method was 19.5 mm. Within this range the mean (standard deviation) mTRE was 3.3(1.6) mm.

IV.C. Intensity-based 2D-3D registration experiments on clinical patient data

The capture range of the 2D-3D intensity-based method was 5.5 mm. The average registration error within this range was 1.62 mm. Registration experiments using the initialized and uninitialized intensity-based method were performed

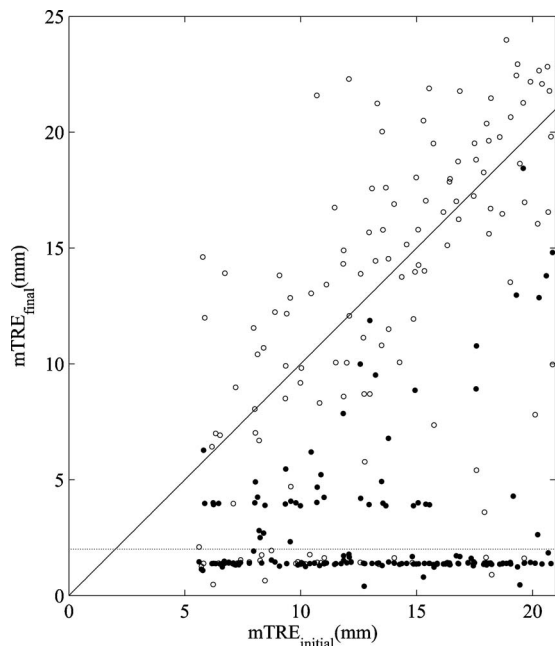


FIG. 8. Results of the intensity-based 2D-3D experiments (C). $mTRE_{final}$ of IBM (open circles) and I-IBM (closed circles) are given as a function of $mTRE_{start}$. The boundary of no improvement and the threshold for success are indicated by the solid and the dashed line, respectively.

with random start positions varying from 5.5 to 21 mm. On average, registration by IBM took ten Powell iterations. The initialization required an average of six iterations to provide an estimate of the transform parameters.

The $mTRE_{final}$ as a function of the $mTRE_{start}$ for IBM (open circles) and I-IBM (closed circles) are presented in Fig. 8. Within this range of $mTRE_{start}$, IBM was successful in 28.8% of the experiments ($n=137$) with an average $mTRE_{final}$ of 11.5 mm. I-IBM had a success percentage of 68.6% and an average $mTRE_{final}$ of 3.1 mm. The figure shows that there is a bias in the $mTRE_{final}$ of approximately 1.3 mm. These biases were nearly all caused by a final translational error along the axis of projection. It should be noted that this bias is a flaw in the 2D-3D registration procedure and was not influenced by the initialization method, whereas a similar bias is seen for registration without initialization. The bias is possibly a result of the very small changes in the registration metric as a function of translations along this axis. IBM could therefore easily get stuck in a local minimum. Another reason could be that the calibration values of the C-arm system contained a slight error. It must be noted that the bias did not influence the results, because the experiments were performed as a comparison.

V. DISCUSSION AND CONCLUSIONS

Although accurate 2D-3D registration methods are available, robustness remains a critical issue for the application of 2D-3D registration for real-time navigation during clinical procedures. We have investigated the feasibility of using the projection-slice theorem and phase correlation to give an estimate of the transform parameters as an initialization for a

2D-3D registration algorithm. With this method, we aim to decrease the mean target registration error to a value that lies within the capture range of existing 2D-3D registration methods.

We evaluated the estimation of the rotational transform parameters with the projection-slice theorem using DRRs generated with cone-beam geometry. For rotational offsets the estimation method showed a capture range of 19.3 mm mTRE, which corresponds to a rotation of 19° – 24° around one axis. For a fixed rotational offset and translational offsets up to 17.3 mm our method provided an improved estimate of rotational transform parameters in all experiments.

Additionally, the method was tested using two sets of x-ray images and their corresponding reconstructed volumes. The overall capture range of our method for these experiments was 19.5 mm mTRE using a single x-ray image, with a mean (standard deviation) mTRE of 3.3 (1.6) mm.

Finally, we have tested the initialization method in combination with an intensity-based 2D-3D registration method. We have shown that for misregistrations in the order of 5.5–21 mm mTRE, registration with initialization succeeded in 68.8% of the experiments, whereas an uninitialized method only led to 28.6% successful experiments.

There are several limitations to the proposed initialization method. The validity of using the projection-slice theorem is limited by the fact that it assumes parallel imaging whereas the projection images acquired during an intervention are generated with cone-beam geometry. In addition, using phase correlation to estimate the translation transform parameters between two images is valid for images that differ only by a relative shift. In our method, we calculate the phase correlation between images that, apart from any translational differences, differ by their projection geometry. Additionally, the orthoscopic projections are obtained using an estimate of the rotational parameters. We have shown, however, that a cone-beam projection with imaging parameters used in clinical practice shows sufficient similarity with its corresponding parallel projection in order for our method to provide an efficient estimate at a lower computational load of $O(N^2 \log N)$ compared to the computation load of the generation of DRRs $O(N^3)$, considering a 3D volume with size $N \times N \times N$.⁶¹ Both intensity-based registration method and the initialization method were implemented using the ITK Segmentation and Registration Toolkit⁵⁷ and were optimized for precision and accuracy and not for speed. For comparison, on average, the IBM took 32.2 min per registration task and the proposed method required 7.5 min per initialization. The runtimes of both algorithms are very unrealistic for clinical applications. However, it has been reported that the generation of DRRs and other registration tasks can easily be accelerated by dedicated programming and hardware implementation on the graphics processing unit.^{39,62,63} For instance, in the experiments (C) the generation of a single DRR with the IBM required 0.7 s. Ruijters *et al.* have shown that with using a similar size data set as the one used in our experiments, DRRs could be generated within 29 ms. We

expect that with similar dedicated programming and hardware implementation, the runtime of the initialization method will be accelerated considerably.

We proposed to use the projection-slice theorem in combination with phase correlation as an estimation method for robust initialization of a 2D-3D registration routine. With the experiments, we have shown that in spite of the ambiguous relation between projection images acquired with cone-beam geometry and the orthoscopic projections, the method provides successful estimates and is able to improve the capture range of a 2D-3D registration method substantially.

^{a)}Electronic mail: m.vanderbom@umcutrecht.nl; Telephone: +31 88 755 6053; Fax: +31 30 251 3399.

¹R. Assaker, P. Cinquin, A. Cotton, and J. P. Lejeune, "Image-guided endoscopic spine surgery, Part 1: A feasibility study," *Spine* **26**(15), 1705–1710 (2001).

²R. Assaker, N. Reyns, B. Pertruzon, and J. P. Lejeune, "Image-guided endoscopic spine surgery, Part 2: Clinical application," *Spine* **26**(15), 1711–1718 (2001).

³E. B. van de Kraats, B. Carelsen, W. J. Fokkens, S. N. Boon, N. Noordhoek, W. J. Niessen, and T. van Walsum, "Direct navigation on 3D rotational x-ray data acquired with a mobile propeller C-arm: Accuracy and application in functional endoscopic sinus surgery," *Phys. Med. Biol.* **50**(24), 5769–5781 (2005).

⁴E. B. van de Kraats, T. van Walsum, L. Kendrick, N. Noordhoek, and W. Niessen, "Accuracy evaluation of direct navigation with an isocentric 3D rotational x-ray system," *Med. Image Anal.* **10**(2), 113–124 (2006).

⁵D. Brandenberger, W. Birkfellner, B. Baumann, P. Messmer, R. W. Huegli, P. Regazzoni, and A. L. Jacob, "Positioning accuracy in a registration-free CT-based navigation system," *Phys. Med. Biol.* **52**(23), 7073–7086 (2007).

⁶C. R. Mascott, "In vivo accuracy of image guidance performed using optical tracking and optimized registration," *J. Neurosurg.* **105**, 561–567 (2006).

⁷L. Lemieux, R. Jagoe, D. R. Fish, N. D. Kitchen, and D. G. T. Thomas, "A patient-to-computed-tomography image registration method based on digitally reconstructed radiographs," *Med. Phys.* **21**(11), 1749–1760 (1994).

⁸S. Lavallée and R. Szeliski, "Recovering the position and orientation of free-form objects from image contours using 3-D distance maps," *IEEE Trans. Pattern Anal. Mach. Intell.* **17**(4), 378–390 (1995).

⁹K. G. A. Gilhuijs, P. J. H. van de Ven, and M. Van Herk, "Automatic three dimensional inspection of patient setup in radiation therapy using portal images, simulator images, and computed tomography data," *Med. Phys.* **23**(3), 389–399 (1996).

¹⁰L. M. G. Brown and T. E. Boulton, "Registration of planar film radiographs with computed tomography," in Proceedings of the IEEE Workshop on Mathematical Methods in Biomedical Image Analysis—MMBIA'96, 1996, pp. 42–51 (unpublished).

¹¹J. Feldmar, N. Ayache, and F. Betting, "3D-2D projective registration of free-form curves and surfaces," *Comput. Vis. Image Underst.* **65**(3), 403–424 (1997).

¹²M. J. Murphy, "An automatic six-degree-of-freedom image registration algorithm for image-guided frameless stereotaxic radiosurgery," *Med. Phys.* **24**(6), 857–866 (1997).

¹³J. Weese, G. P. Penney, P. Desmedt, T. M. Buzug, D. L. Hill, and D. J. Hawkes, "Voxel-based 2-D/3-D registration of fluoroscopy images and CT scans for image-guided surgery," *IEEE Trans. Inf. Technol. Biomed.* **1**(4), 284–293 (1997).

¹⁴A. Guézic, P. Kazanzides, B. Williamson, and R. H. Taylor, "Anatomy based registration of CT-scan and intraoperative x-ray images for guiding a surgical robot," *IEEE Trans. Med. Imaging* **17**(5), 715–728 (1998).

¹⁵A. Liu, E. Bullitt, and S. M. Pizer, "3D/2D registration via skeletal near projective invariance in tubular objects," in Proceedings of Medical Image Computing and Computer-Assisted Interventions—MICCAI'98, 1998 [Lect. Notes Comput. Sci. **1496**, 952–963 (1998)].

¹⁶Y. Kita, D. L. Wilson, and J. A. Noble, "Real-time registration of 3D cerebral vessels to x-ray angiograms," in Proceedings of Medical Image Computing and Computer-Assisted Interventions—MICCAI'98, 1998

[Lect. Notes Comput. Sci. **1496**, 1125–1133 (1998)].

¹⁷C. R. Maurer, Jr., R. J. Maciunas, and J. M. Fitzpatrick, "Registration of head CT images to physical space using a weighted combination of points and surfaces," *IEEE Trans. Med. Imaging* **17**(5), 753–761 (1998).

¹⁸G. P. Penney, J. Weese, J. A. Little, P. Desmedt, D. L. G. Hill, and D. J. Hawkes, "A comparison of similarity measures for use in 2-D-3D medical image registration," *IEEE Trans. Med. Imaging* **17**(4), 586–595 (1998).

¹⁹A. Hamadeh, S. Lavallee, and P. Cinquin, "Automated 3-dimensional computed tomographic and fluoroscopic image registration," *Comput. Aided Surg.* **3**(1), 11–19 (1998).

²⁰L. M. Sirois, D. H. Hristov, and B. G. Fallone, "Three-dimensional anatomy setup verification by correlation of orthogonal portal images and digitally reconstructed radiographs," *Med. Phys.* **26**(11), 2422–2428 (1999).

²¹G. P. Penney, P. G. Batchelor, D. L. Hill, and D. J. Hawkes, "Validation of a two-to three-dimensional registration algorithm for aligning preoperative CT images and intraoperative fluoroscopy images," *Med. Phys.* **28**(6), 1024–1032 (2001).

²²J. Kim, J. A. Fessler, K. L. Lam, J. M. Balter, and R. K. Ten Haken, "A feasibility study of mutual information based setup error estimation for radiotherapy," *Med. Phys.* **28**(12), 2507–2517 (2001).

²³S. Clippe, D. Sarut, C. Malet, S. Miguot, C. Ginestet, and C. Carrie, "Patient setup error measurement using 3D intensity-based image registration techniques," *Int. J. Radiat. Oncol., Biol., Phys.* **56**(1), 259–265 (2003).

²⁴D. Tomažević, B. Likar, T. Slivnik, and F. Pernuš, "3-D/2-D registration of CT and MR to x-ray images," *IEEE Trans. Med. Imaging* **22**(11), 1407–1416 (2003).

²⁵H. Livyatan, Z. Yaniv, and L. Joskowicz, "Gradient-based 2-D/3-D rigid registration of fluoroscopic x-ray to CT," *IEEE Trans. Med. Imaging* **22**(11), 1395–1406 (2003).

²⁶W. Birkfellner, J. Wirth, W. Burgstaller, B. Baumann, H. Staedele, B. Hammer, N. C. Gellrich, A. L. Jacob, P. Regazzoni, and P. Messmer, "A faster method for 3D/2D medical image registration—A simulation study," *Phys. Med. Biol.* **48**(16), 2665–2679 (2003).

²⁷S. Benamer, M. Mignotte, S. Parent, H. Labelle, W. Skalli, and J. de Guise, "3D/2D registration of scoliotic vertebrae using statistical models," *Comput. Med. Imaging Graph.* **27**(5), 321–337 (2003).

²⁸J. H. Hipwell, G. P. Penney, R. A. McLaughlin, K. Rhode, P. Summers, T. C. Cox, J. V. Byrne, J. A. Noble, and D. J. Hawkes, "Intensity-based 2-D-3-D registration of cerebral angiograms," *IEEE Trans. Med. Imaging* **22**(11), 1417–1426 (2003).

²⁹R. Bansal, L. H. Staib, Z. Chen, A. Rangarajan, J. Knisely, R. Nath, and J. S. Duncan, "Entropy-based dual-portal-to-3-DCT registration incorporating pixel correlation," *IEEE Trans. Med. Imaging* **22**(1), 29–49 (2003).

³⁰J. Kim, S. D. Li, D. Pradhan, R. Hammoud, Q. Chen, F. F. Yin, Y. Zhao, J. H. Kim, and B. Movsas, "Effects of x-ray and CT image enhancements on the robustness and accuracy of a rigid 3D/2D image registration," *Med. Phys.* **32**(4), 866–873 (2005).

³¹T. Rohlfing, D. B. Russakoff, J. Denzler, K. Mori, and C. R. Maurer, "Progressive attenuation fields: Fast 2D-3D image registration without precomputation," *Med. Phys.* **32**(9), 2870–2880 (2005).

³²D. B. Russakoff, T. Rohlfing, K. Mori, D. Rueckert, A. Ho, J. R. Adler, and C. R. Maurer, "Fast generation of digitally reconstructed radiographs using attenuation fields with application to 2D-3D image registration," *IEEE Trans. Med. Imaging* **24**(11), 1441–1454 (2005).

³³G. A. Turgeon, G. Lehmann, G. Guiraudon, M. Drangova, D. Holdsworth, and T. Peters, "2D-3D registration of coronary angiograms for cardiac procedure planning and guidance," *Med. Phys.* **32**(12), 3737–3749 (2005).

³⁴R. A. McLaughlin, J. Hipwell, D. J. Hawkes, J. A. Noble, J. V. Byrne, and T. C. Cox, "A comparison of a similarity-based and a feature-based 2-D-3-D registration method for neurointerventional use," *IEEE Trans. Med. Imaging* **24**(8), 1058–1066 (2005).

³⁵H.-S. Jans and A. M. Syme, "3D interfractional patient position verification using 2D-3D registration of orthogonal images," *Med. Phys.* **33**(5), 1420–1439 (2006).

³⁶J. Y. Jin, S. Ryu, K. Faber, T. Mikkelsen, Q. Chen, S. D. Li, and B. Movsas, "2D/3D image fusion for accurate target localization and evaluation of a mask based stereotactic system in fractionated stereotactic radiotherapy of cranial lesions," *Med. Phys.* **33**(12), 4557–4566 (2006).

³⁷D. Tomažević, B. Likar, and F. Pernuš, "3-D/2-D registration by integrating 2-D information in 3-D," *IEEE Trans. Med. Imaging* **25**(1), 17–27

- (2006).
- ³⁸J. Dey and S. Napel, "Targeted 2D/3D registration using ray normalization and a hybrid optimizer," *Med. Phys.* **33**(12), 4730–4735 (2006).
 - ³⁹A. Khamene, P. Bloch, W. Wein, M. Svatos, and F. Sauer, "Automatic registration of portal images and volumetric CT for patient positioning in radiation therapy," *Med. Image Anal.* **10**(1), 96–112 (2006).
 - ⁴⁰R. Munbodh, Z. Chen, D. A. Jaffray, D. J. Moseley, J. P. S. Knisely, and J. S. Duncan, "Automated 2D-3D registration of radiograph and a cone beam CT using line-segment enhancement," *Med. Phys.* **33**(5), 1398–1411 (2006).
 - ⁴¹L. L. Chen, T. B. Jones, E. Jones, Z. Q. Chen, W. Luo, L. Wang, R. A. Price, A. Pollack, and C. A. C. Ma, "Magnetic resonance-based treatment planning for prostate intensity-modulated radiotherapy: Reconstruction of digitally reconstructed radiographs," *Int. J. Radiat. Oncol. Biol., Phys.* **68**(3), 903–911 (2007).
 - ⁴²R. Munbodh, Z. Chen, D. A. Jaffray, D. J. Moseley, J. P. S. Knisely, and J. S. Duncan, "A frequency-based approach to locate common structure for 2D-3D intensity-based registration of setup images in prostate radiotherapy," *Med. Phys.* **34**(7), 3005–3017 (2007).
 - ⁴³S. Aouadi and L. Sarry, "Accurate and precise 2D-3D registration based on x-ray intensity," *Comput. Vis. Image Underst.* **110**(1), 134–151 (2008).
 - ⁴⁴X. Chen, M. R. Varley, L. K. Shark, G. S. Shentall, and M. C. Kirby, "A computationally efficient method for automatic registration of orthogonal x-ray images with volumetric CT data," *Phys. Med. Biol.* **53**(4), 967–983 (2008).
 - ⁴⁵D. S. Fu and G. Kuduvali, "A fast, accurate, and automatic 2D-3D image registration for image-guided cranial radiosurgery," *Med. Phys.* **35**(5), 2180–2194 (2008).
 - ⁴⁶P. Markelj, D. Tomaževič, and F. Pernuš, "Robust gradient-based 3-D/2-D registration of CT and MR to X-ray images," *IEEE Trans. Med. Imaging* **27**(12), 1704–1714 (2008).
 - ⁴⁷E. van de Kraats, G. P. Penney, D. Tomaževič, T. van Walsum, and W. Niessen, "Standardized evaluation methodology for 2D-3D registration," *IEEE Trans. Med. Imaging* **24**(9), 1177–1189 (2005).
 - ⁴⁸E. De Castro and C. Morandi, "Registration of translated and rotated images using finite Fourier transforms," *IEEE Trans. Pattern Anal. Mach. Intell.* **PAMI-9**(5), 700–703 (1987).
 - ⁴⁹A. Kassam and M. L. Wood, "Fourier registration of three-dimensional brain MR images: Exploiting the axis of rotation," *J. Magn. Reson Imaging* **6**(6), 894–902 (1996).
 - ⁵⁰C. D. Kuglin and D. C. Hines, "The phase correlation image alignment method," in *Proceedings of the IEEE 1975 Conference on Cybernetics and Society*, 1975, pp. 163–165 (unpublished).
 - ⁵¹J. L. Horner and P. D. Gianino, "Phase-only matched filtering," *Appl. Opt.* **23**(6), 812–816 (1984).
 - ⁵²M. J. van der Bom, J. P. W. Pluim, R. Homan, J. Timmer, and L. W. Bartels, "Projection-slice theorem based 2D-3D registration," in *SPIE Medical Imaging: Imaging Processing*, edited by J. M. Reinhardt and J. P. W. Pluim, SPIE Press, Bellingham, 2007, Vol. 6512, p. 65120B.
 - ⁵³D. Zosso, B. Le Calennec, M. Bach Cuadra, K. Aminian, B. M. Jolles, and J. P. Thiran, "Bi-planar 2D-to-3D registration in Fourier domain for stereoscopic x-ray motion tracking," in *SPIE Medical Imaging: Imaging Processing*, edited by J. M. Reinhardt and J. P. W. Pluim, SPIE Press, Bellingham, 2008, Vol. 6914, p. 69140I.
 - ⁵⁴D. Gottlieb, B. Gustafsson, and P. Forssén, "On the direct Fourier method for computer tomography," *IEEE Trans. Med. Imaging* **19**(3), 223–232 (2000).
 - ⁵⁵F. Natterer, *The Mathematics of Computerized Tomography* (B.G. Teubner, Stuttgart, 1986).
 - ⁵⁶M. J. D. Powell, "An efficient method for finding the minimum of a function of several variables without calculating derivatives," *Comput. J.* **7**(2), 155–162 (1964).
 - ⁵⁷L. Ibáñez, W. Schroeder, L. Ng, and J. Cates, *The ITK Software Guide*, 2nd ed. (Kitware Inc., Clifton Park, 2005).
 - ⁵⁸J. M. Fitzpatrick, J. B. West, and C. R. Maurer, "Predicting error in rigid-body point-based registration," *IEEE Trans. Med. Imaging* **17**(5), 694–702 (1998).
 - ⁵⁹S. Klein, M. Staring, K. Murphy, M. A. Viergever, and J. P. W. Pluim, "Elastix: A toolbox for intensity-based medical image registration," *IEEE Trans. Image Process.* **29**(1), 196–205 (2010).
 - ⁶⁰L. Li and M. K. H. Leung, "Integrating intensity and texture differences for robust change detection," *IEEE Trans. Image Process.* **11**(2), 105–112 (2002).
 - ⁶¹E. Ntasis, T. A. Maniatis, and K. S. Nikita, "Fourier volume rendering for real time preview of digital reconstructed radiographs: A web-based implementation," *Comput. Med. Imaging Graph.* **26**(1), 1–8 (2002).
 - ⁶²D. Ruijters, B. M. ter Haar Romeny, and P. Suetens, "GPU-accelerated digitally reconstructed radiographs," in *Biomedical 2008*, edited by A. Hierlemann, ACTA Press, Calgary, AB, Canada, 2008 Vol. 601, p. 041.
 - ⁶³D. Ruijters, B. M. ter Haar Romeny, and P. Suetens, "Efficient GPU-accelerated elastic image registration," in *Biomedical Engineering, BioMED 2008*, edited by A. Hierlemann, ACTA Press, Calgary, AB, Canada, 2008 Vol. 601, p. 027.